Marine ice recycling at the southern McMurdo Ice Shelf, Antarctica

Inka KOCH,[1] Sean FITZSIMONS,[1] Denis SAMYN,[2] Jean-Louis TISON[3]

[1]*Department of Geography, University of Otago, Dunedin, New Zealand*
[2]*Department of Mechanical Engineering, Nagaoka University of Technology, Nagaoka, Niigata, Japan*
[3]*Laboratoire de Glaciologie, Université Libre de Bruxelles, Brussels, Belgium*
Correspondence: I. Koch <inkakoch@gmail.com>

ABSTRACT. Marine ice accretes at the base of ice shelves, often infilling open structural weaknesses and increasing ice-shelf stability. However, the timing and location of marine ice formation remain poorly understood. This study determines marine ice source water composition and origin by examining marine ice crystal morphology, water isotope and solute chemistry in ice samples collected from the southern McMurdo Ice Shelf (SMIS), Antarctica. The measured co-isotopic record together with the output of a freezing model for frazil crystals indicate a spatio-temporally varying water source of sea water and relatively fresher water, such as melted meteoric or marine ice. This is in agreement with the occurrence of primarily banded and granular ice crystal facies typical for frazil ice crystals that nucleate in a supercooled mixture of water masses. We propose that marine ice exposed at the surface of SMIS, which experiences summer melt, is routed to the ice-shelf base via the tide crack. Here frazil crystals nucleate in a double diffusion mechanism of heat and salt between two water masses at their salinity-dependent freezing point. Recycling of previously formed marine ice facilitates ice-shelf self-sustenance in a warming climate.

KEYWORDS: Antarctic glaciology, ice chemistry, ice crystal studies, ice shelves, ice/ocean interactions

INTRODUCTION

Marine ice forms from a mixture of sea and fresh water and adds mass to the underside of ice shelves. It can accrete in open basal structures, such as rifts and crevasses (Morgan, 1972; Souchez and others, 1991; Oerter and others, 1992; Tison and others, 1993; Eicken, 1994; Khazendar and others, 2001; Craven and others, 2004, 2009; Pattyn and others, 2012; Jansen and others, 2013), suture zones (Jansen and others, 2013; Kulessa and others, 2014) or as a massive layer below meteoric ice-shelf ice (Zotikov and others, 1980; Craven and others, 2009; Treverrow and others, 2010). Its presence influences the rheology and stability of ice shelves (Khazendar and others, 2009; Kulessa and others, 2014), which drain 74% of Antarctica's grounded ice together with outlet glaciers (Bindschadler and others, 2011). Ice shelves also buttress most ice streams (Dupont and Alley, 2005). Marine ice has been increasingly observed in Antarctic ice shelves, either directly in ice-core samples (Zotikov and others, 1980; Souchez and others, 1991; Tison and others, 1993; Eicken and others, 1994; Khazendar and others, 2001; Craven and others, 2009; Pattyn and others, 2012; Dierckx and others, 2014) or remotely using geophysical methods (Fricker and others, 2001; Joughin and Vaughan, 2004; McMahon and Lackie, 2006; Khazendar and others, 2009; Pattyn and others, 2012; Jansen and others, 2013).

Due to the difficulty associated with accessing the ice-shelf cavity, processes of marine ice formation, including timing, location and volume, remain largely unknown. Since marine ice can be several hundred metres thick (e.g. Amery Ice Shelf, East Antarctica; Craven and others, 2009), fast-forming frazil ice crystals are assumed to be mainly responsible for the generation of marine ice (Treverrow and others, 2010), allowing for marine ice accumulation rates of $>1\ \mathrm{m\,a^{-1}}$ at some ice shelves (Bombosch and Jenkins, 1995; Wen and others, 2010). Indeed, loose agglomerations of frazil ice crystals have been observed below ice shelves in borehole imagery (Craven and others, 2005; Hubbard and others, 2012). These small freely floating discoid ice crystals nucleate in supercooled water (Martin, 1981; Daly, 1984), which is water cooled below its in situ freezing point without changing state (Leonard and others, 2014). Supercooling of water masses below ice shelves can occur as a result of a change in the pressure-dependent freezing point due to adiabatically rising water masses (Foldvik and Kvinge, 1974) or double diffusion of heat and salt between water masses of different salinities at their freezing point (Souchez and others, 1998). Both mechanisms generally involve mixing of sea water with fresher water. The former process is part of a thermohaline circulation often referred to as the 'ice pump' mechanism (Lewis and Perkin, 1986) and has been widely associated with marine ice formation in thick layers (e.g. Galton-Fenzi and others, 2012). Hereby, continental freshwater ice is melted at depth close to the grounding line of an ice shelf by denser High Salinity Shelf Water (HSSW), which is generated during sea-ice formation in winter. Similarly, warmer Circumpolar Deep Water (CDW) can enter the ice-shelf cavity inducing melt at the ice-shelf base (Jacobs and others, 1992). This meltwater then rises along the gradient of the ice shelf due to its buoyancy to shallower waters, where it becomes supercooled due to a change in the pressure-dependent freezing point and frazil ice crystals nucleate (Galton-Fenzi and others, 2012). Double diffusion-induced supercooling could occur close to the grounding line of shallower ice shelves, where surface meltwater can percolate through sediment (Souchez and others, 1998) or drain through tide cracks (Gow and others, 1965; Gow and Epstein, 1972) to the ice/water interface. Heat diffuses faster than salt from relatively

https://doi.org/10.3189/2015JoG14J095 Published online by Cambridge University Press

Table 1. Occurrence of ice crystal facies (gr: granular; bd: banded; clm: columnar; pl: platelet), measured range in $\delta^{18}O$ and salinity, and co-isotopic slopes of marine ice in previous studies

Ice shelf	Ice crystals	$\delta^{18}O$ ‰	Salinity ‰	Co-isotopic slope	Source
Amery Ice Shelf	–	0.00 to 2.30	~0.02		Morgan (1972), cited in Goodwin (1993)
Amery Ice Shelf	gr, bd	–0.60 to 1.50	0.06 to 0.75	–	Craven and others (2004)
Amery Ice Shelf	gr, bd	–	–	–	Treverrow and others (2010)
Campbell Glacier Tongue	gr	–17.00 to ~1.00	–	7.86 ($r = 0.998$)	Souchez and others (1995)
Filchner–Ronne Ice Shelf	gr	~2.00	<0.10	–	Oerter and others (1992)
Filchner–Ronne Ice Shelf	gr	–	0.02 to 0.10	–	Eicken (1994)
Hell's Gate Ice Shelf	clm, pl, gr	1.00 to 3.20	0.01 to 0.80 (Na content only)	6.60 ($r = 0.93$, marine ice + sea-water samples)	Souchez and others (1991)
Hell's Gate Ice Shelf	clm, pl, gr, bd	1.14 to 3.26	0.03 to 1.42	–	Tison and others (1993)
Hell's Gate Ice Shelf	clm	1.14 to 2.02	1.35	–	Tison and others (1993)
Hell's Gate Ice Shelf	pl	2.08 to 2.51	1.42	–	Tison and others (1993)
Hell's Gate Ice Shelf	gr	1.82 to 3.26	0.03 to 0.14	–	Tison and others (1993)
Hell's Gate Ice Shelf	bd	1.64 to 3.02	0.19 to 0.36	–	Tison and others (1993)
Hell's Gate Ice Shelf	–	~–15.00 to –3.00	–	7.71 ($r = 0.99$)	Souchez and others (1998)
Koettlitz Ice Tongue	pl	1.37 to 2.51	0.20 to 5.26	–	Gow and Epstein (1972)
Law Dome – type 1 marine ice	clm	0.26 to 1.56	0.01 to 0.08 (Na content only)	8.10	Goodwin (1993)
Law Dome – type 2 marine ice	gr	–16.93 to –2.57	0.01 to 0.08 (Na content only)	7.80	Goodwin (1993)
Northern McMurdo Ice Shelf	gr	–	~0.01 to ~0.90	–	Gow and others (1965)
Southern McMurdo Ice Shelf	–	–2.80 to 2.90	–	–	Kellogg and others (1991a,b)
Southern McMurdo Ice Shelf	–	~–4.40 to ~2.50	–	7.82 ($r = 0.99$, mix of meteoric and marine ice)	Fitzsimons and others (2012)
Nansen Ice Shelf	gr, bd	1.80 to 2.37	0.04 to 0.15	–	Khazendar and others (2001)
Hell's Gate Ice Shelf	gr, bd	–	0.03 to 0.23 (inferred from Cl measurements)	–	Dierckx and others (2013, 2014)
Ross Ice Shelf	clm	–	~2.00 to ~4.00	–	Zotikov and others (1980)
Roi Baudouin Ice Shelf rift	gr, bd	~0.00 to ~2.20	~0.03 to ~9.20	–	Pattyn and others (2012)

warmer meltwater to colder sea water (Martin and Kauffman, 1974). This results in rapid freezing of the less saline water mass. If both water masses are near their salinity-dependent freezing point and become turbulently mixed, frazil ice crystals might nucleate in a double diffusion process (McPhee and others, 2013). This could be driven by a shallow tidal circulation. If supercooled water extends to the ocean floor, frazil ice crystals can also flock together on the sea floor, forming anchor ice (Mager and others, 2013). This ice could eventually lift off the ocean floor when its buoyancy is large enough and contribute to marine ice at the ice-shelf base (e.g. Swithinbank, 1970).

Over time, frazil ice crystals gradually sinter together and adjust their shape to minimize the surface energy of the ice crystals (Martin, 1981). However, it remains uncertain whether marine ice is formed from frazil ice crystals only, that grow, settle and compact much like snow due to the buoyancy pressure, or whether 'pore spaces' between individual frazil ice crystals are filled by sea water, which freezes as a result of heat conduction through the ice shelf (Eicken, 1994; Tison and others, 2001). In either case, the bulk of marine ice (70–95%) would be made up of frazil ice crystals due to their high buoyancy pressure (Tison and others, 2001). Once consolidated, frazil ice crystals in marine ice form granular, banded or platelet ice facies. Granular ice facies have been observed most frequently in marine ice formed from primarily frazil ice crystals (Oerter and others, 1992; Tison and others, 1993; Eicken and others, 1994; Treverrow and others, 2010), followed by banded ice facies (Khazendar and others, 2001; Craven and others, 2004; Tison and others, 2010; Treverrow and others, 2010; Pattyn and others, 2012) (Table 1). Large platelet ice facies are less common in marine ice (Gow and Epstein, 1972; Tison and others, 1993) (Table 1).

A better understanding of marine ice formation processes outlined above contributes to the assessment of the stability of ice shelves, many of which are experiencing rapid change as a result of increased ice-shelf basal melt rates due to oceanic erosion (e.g. Depoorter and others, 2013) and surface melt/ponding (e.g. Banwell and others, 2014). The aim of this study is to determine the composition and origin of water masses that freeze to form marine ice at the southern McMurdo Ice Shelf (SMIS), Antarctica, (Fig. 1) and whether there are spatio-temporal variations. To accomplish this, marine ice samples were collected from different SMIS sites, and the ice crystal morphology and chemistry was analysed in conjunction with a boundary layer freezing model. The data are interpreted in the light of the geographic setting to determine whether marine ice at SMIS was formed as a result of a deep thermohaline circulation, or in a double diffusion mechanism of heat and salt during turbulent mixing of sea water with fresher surface meltwater.

SAMPLING AND DATA ANALYSIS

In this section we describe the field site and give a summary of previous studies. We also detail marine ice extraction from the ice shelf and its laboratory analysis for water

https://doi.org/10.3189/2015JoG14J095 Published online by Cambridge University Press

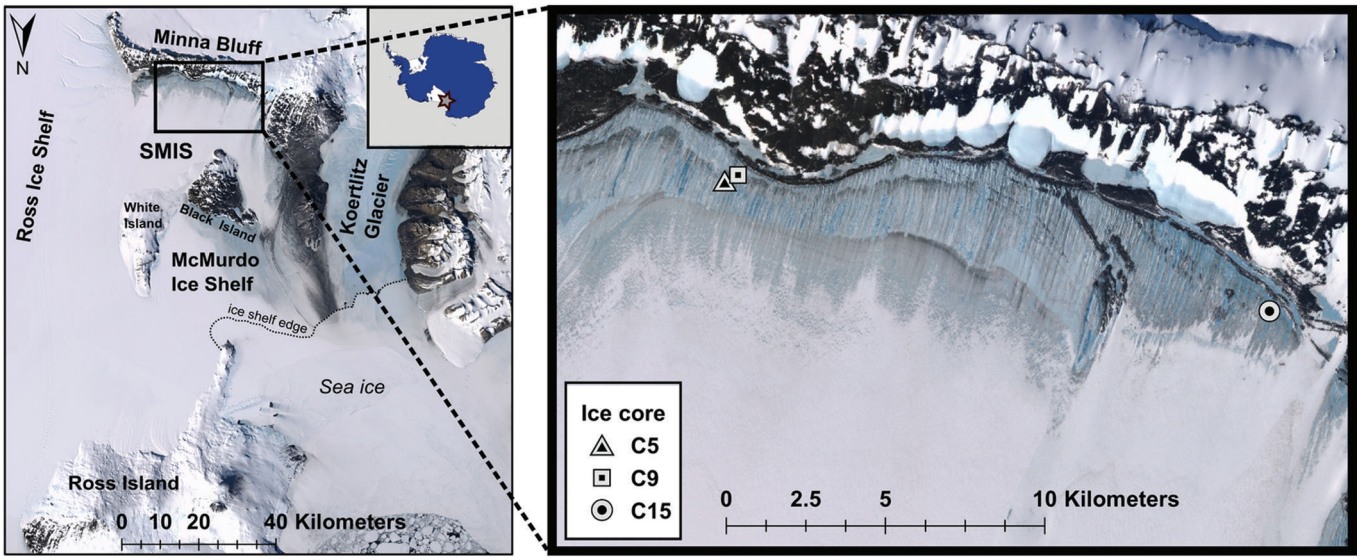

Fig. 1. Landsat Image Mosaic of Antarctica (LIMA) showing the location of the southern McMurdo Ice Shelf (SMIS), McMurdo Sound, Antarctica. Inset shows a detailed view of the marine ice sampling sites close to Minna Bluff. Marine ice occurs in a zone of relatively darker ice at SMIS, which is separated from the lighter meteoric ice by a distinct boundary running parallel to shore (2–3.5 km from shore) (see Fitzsimons and others, 2012, fig. 1).

isotope and major ion composition. The frazil ice boundary-layer freezing model, which is used to compare theoretical and measured water isotope signals of marine ice, is explained below. Thin sectioning of marine ice and the classification of ice crystal morphology into different ice facies are also described.

Field site

SMIS is a small ice shelf ($\sim 30 \times 35\,km^2$) in Antarctica confined by Minna Bluff to the south and Black and White Islands to the north (Fig. 1). It is separated from the much larger and two magnitudes faster-flowing Ross Ice Shelf by a rift zone (Fig. 1). SMIS flows slowly at a rate of 0.4–7.3 m a^{-1} in a west-southwesterly direction toward Minna Bluff in its southern parts and in a west-northwesterly direction in its northwestern parts (Clifford, 2005). The ice shelf floats on a water column of 300–400 m in its centre (Johnston and others, 2008). Ground-penetrating and airborne radar investigations have revealed that the ice shelf is thickest in the north (~180 m) and thins (to ~100 m) toward its eastern and southern margins (Swithinbank, 1970; Clifford, 2005), where the radar signal becomes lost 5–6 km from shore. This was ascribed to outcropping of slightly saline marine ice at the snow-free ice-shelf surface close to the shore of Minna Bluff (Fig. 1) (Clifford, 2005). The presence of marine ice was also detected in previous studies on ice composition (Kellogg and others, 1991a; Fitzsimons and others, 2012) and inferred from the presence of marine macrofossils at the ice-shelf surface (Debenham, 1919; Gow and others, 1965; Swithinbank, 1970; Kellogg and others, 1990, 1991b; Fitzsimons and others, 2012). Two of these shells were radiocarbon-dated to 1230 ± 50 and 2850 ± 30 radiocarbon years BP (Kellogg and others, 1990; Denton and Marchant, 2000) using an Antarctic reservoir correction of 1300 years (Berkman and Forman, 1996). However, their age does not necessarily reflect the date of marine ice accretion, since the time of death of the marine organisms is not necessarily related to their entrainment date (Fitzsimons, 1997). Surfacing of marine ice, which was originally accreted at SMIS's base, is speculated to be a result of stripping by katabatic winds (Clifford, 2005), as at the Hell's Gate Ice Shelf (Tison and others, 1993). Modelled wind fields indeed show elevated wind speeds over the southern part of SMIS (Monaghan and others, 2005). Local summer surface melting also contributes to the observed negative surface mass balance (>0.10 m; Clifford, 2005) in the snow-free band running parallel to Minna Bluff (Fig. 1). Melting is likely partially induced by the locally high debris concentration on the ice-shelf surface close to Minna Bluff (Denton and Marchant, 2000) and the lower surface albedo of the darker marine ice (Warren and others, 1997). Surface meltwater pools in several ice-shelf surface lakes (Clifford, 2005), which are often elongated and oriented at right angles to shore (Fig. 2) parallel to the prevailing wind direction (Swithinbank, 1970). These lakes were observed to form in summer, while the rest of the year they were frozen over into 'mirror-smooth' surfaces of ice (Swithinbank, 1970). The lakes are estimated to be ~1 m deep, similar to lakes observed on other ice shelves (e.g. Banwell and others, 2014), several tens to hundreds of metres wide and up to 1–2 km long. Some lakes were observed to drain completely during the course of the melt season.

Ice sampling in the field

Marine ice was extracted in shallow cores from the apex of snow-free ~6 m high ice ridges that separate surficial lakes and are oriented at right angles to shore, almost in a perfect north–south direction (Fig. 2). Cores were taken in November 2010 with a Kovacs corer, and in December 2007 with a custom-made SIPRE-type coring auger. The extracted three ice cores (C5, C9 and C15; Fig. 1) were 2.71 ± 0.01 m, 3.04 ± 0.01 m and 9.49 ± 0.01 m long. The freeboard level was not reached during ice-core extraction since the ice shelf is ≥100 m thick (Clifford, 2005). The top 0.50 ± 0.01 m of every core was discarded to avoid the influence of potential surface melt (Tison and others, 1993). Ice cores were immediately put in a freezer and kept below –15°C during transport and storage.

https://doi.org/10.3189/2015JoG14J095 Published online by Cambridge University Press

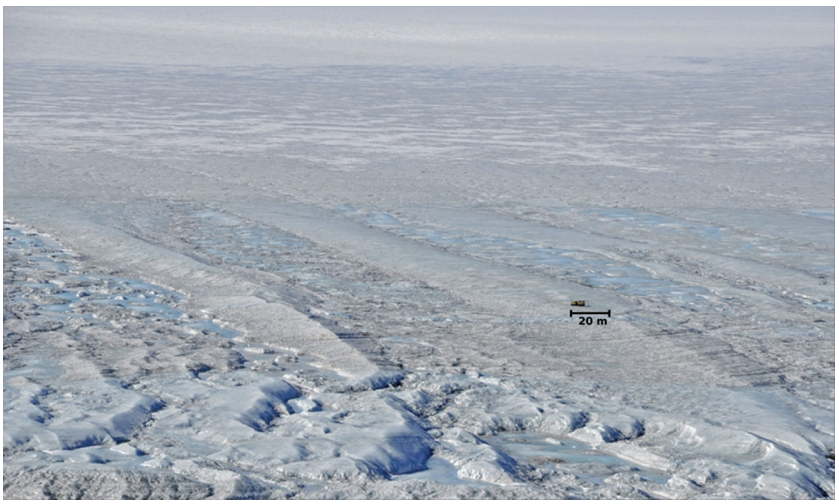

Fig. 2. Marine ice exposed at the ice-shelf surface of SMIS. Photograph was taken in November from Minna Bluff, looking northeast. The Hagglunds vehicle is 7 m long and parked on an ice ridge ~6 m high. Meltwater was observed to pool in elongated ponds between the ridges in December 2010. (Photo: Michael Hambrey.)

Solutes and water isotopes

Ice cores were cut into 0.10 ± 0.001 m sections along the length of the cores and a 0.0075 ± 0.0025 m thick outside rim of the ice cores was cut off to avoid contamination. Subsequently the samples were allowed to melt in closed plastic containers at room temperature. Water samples were filtered under vacuum using MF-Millipore 0.45 µm membrane cellulose acetate and cellulose nitrate filters. The samples were analysed using a Dionex ICS-3000 ion chromatograph to determine the concentration of major cations and anions (Li^+, Na^+, Mg^{2+}, K^+, Ca^{2+}, NH^{4+} and Cl^-, NO^{2-}, Br^-, $NO_3{}^{2-}$, $SO_4{}^{2-}$). A carbonate removal device (CRD-200) was installed to remove the carbonate peak. Precision and accuracy of cation and anion concentrations are better than 5%. The sum of all cations and anions gives the total dissolved solids (TDS), which are quoted in parts per thousand (‰) to allow for easy comparison with salinity measurements of other studies. Ions were measured in mg L^{-1} and are quoted with respect to Standard Mean Ocean Water (SMOW) ion ratios according to Maus and others (2011) (e.g. $\Delta Mg/Cl = (Mg/Cl - (Mg/Cl)_{SMOW})/(Mg/Cl)_{SMOW}$), in which the SMOW ratios were taken from Millero and others (2008). Since individual frazil ice crystals are thought to expel all salt during their formation (Tison and others, 2001), salt could only be included in the pore spaces of the agglomeration or at grain boundaries. Tison and others (1993) suggest that ion fractionation in marine ice is further evidence of the presence of sea-water filled pores, which consolidate slowly, allowing for the selective incorporation of ions. Previous studies have interpreted variations in ion ratios to result from changes in the consolidation rate of marine ice (Oerter and others, 1992; Tison and others, 1993; Moore and others, 1994).

The relative concentration of oxygen and deuterium isotopes ($\delta^{18}O$ and δD) was measured with a Picarro laser spectrometer relative to SMOW (e.g. $\delta^{18}O = \left(\left({}^{18}O/{}^{16}O - ({}^{18}O/{}^{16}O)_{SMOW}\right)/({}^{18}O/{}^{16}O)_{SMOW}\right) \times 1000$). The samples were repeat-injected eight times whereby the first three injections from one sample were discarded due to carry-over from previous samples. The measurement precision was 0.07‰ for $\delta^{18}O$ and 0.40‰ for δD. In order to establish whether marine ice at SMIS was formed from a constant or a changing mixed water source, the regression slope of co-isotopic plots of $\delta^{18}O$ and δD was established and compared to co-isotopic freezing slopes (Souchez and Jouzel, 1984) and mixing slopes (Souchez and Groote, 1985) models. Regression slopes in mixing models are ~8 (Souchez and Groote, 1985), whereas freezing models have smaller slopes (Souchez and Jouzel, 1984) whereby the exact slope magnitude depends on the isotopic composition of the water source. Data trends and interrelations are assessed with the Pearson's product-moment correlation coefficient and are expressed in terms of r. All r values quoted in this paper are significant at the 99% level.

Ice crystal facies

Thin sections of ice were prepared according to the method detailed by Durand and others (2006) vertically along the full length of the ice cores to a thickness of $\sim 0.5 \times 10^{-3}$ m using a conventional biological microtome in a cold room maintained at –15°C. Thin sections were photographed between cross-polarized light, and ice crystals were classified into different ice facies (granular, banded and platelet) based on their shape (Table 2) for every 0.10 m down-core coinciding with the sampling for the ice chemistry. Where 30–70% of both banded and granular ice crystals were present in a 0.10 m long section of thin sections, the ice facies were classified as a mixed ice facies. On the rare occasions when the ice crystal morphology did not fit any of the descriptions, they were logged as 'other'. Ice crystal morphology, as apparent in thin section, is analysed in conjunction with ice chemistry in order to determine whether variations in marine ice source water lead to changes in the appearance of marine ice crystals.

Freezing model for frazil ice crystals

The isotopic source water composition for marine ice predominantly formed by frazil ice crystals can be derived by applying a modelled effective fractionation coefficient (α_{eff}) to the measured isotopic concentration of the ice. This coefficient was calculated using Tison and others' (2001) boundary layer freezing model for individual marine ice

https://doi.org/10.3189/2015JoG14J095 Published online by Cambridge University Press

Table 2. Criteria for the classification of ice crystal facies with examples

Ice crystal facies	Individual grain shape	Grain boundaries	Crystal size (approx.) mm
Banded	Elongated, often rectangular, sometimes acicular	Polygonal with square edges, often diffuse	0.5–30.0
Granular	Isometric and orbicular	Polygonal, interlobate	0.5–20.0
Platelet	Elongated, wider in the middle, thinner toward the edges, sometimes acicular	Interlobate	10.0–50.0

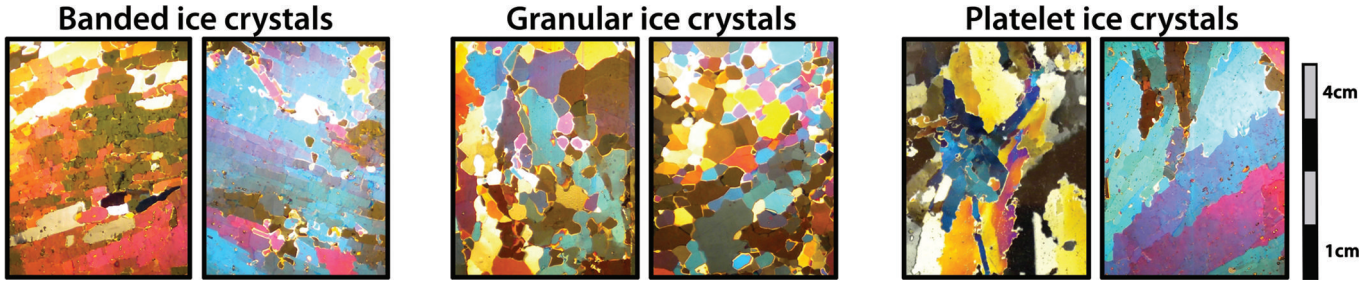

frazil ice crystals. The model is based upon Burton and others' (1953) boundary layer model originally developed for simulating solute diffusion into a liquid boundary layer during the solidification of metal:

$$\alpha_{\mathrm{eff}} = \frac{\alpha_{\mathrm{equ}}}{\alpha_{\mathrm{equ}} - \left(\alpha_{\mathrm{equ}} - 1\right) \exp\left(\frac{-z_{\mathrm{bl}} V}{D}\right)} \quad (1)$$

where the effective fractionation coefficient (α_{eff}; unitless) is calculated from the equilibrium fractionation coefficient (α_{equ}; unitless) as a function of the growth rate (v; m s^{-1}), diffusion coefficient (D; m^2 s^{-1}) and boundary layer thickness (z_{bl}; m). The isotopic concentration (c; unitless) in the boundary layer near the ice/water interface hereby changes over time (t; s) according to Fick's law (Burton and others, 1953; Eicken, 1998):

$$\frac{\partial c}{\partial t} = D\frac{\partial^2 c}{\partial z^2} + V\frac{\partial c}{\partial z} \quad (2)$$

where z is the distance from the ice/water interface into the fluid (m) and V is the freezing velocity of the ice front (m s^{-1}). The model is run with a Crank–Nicolson scheme to allow for simultaneous diffusion and fractionation during the advancement of a freezing front. In the model, water is frozen from a semi-infinite reservoir (basically assuming an open system). Tison and others (2001) used a simple rod geometry for frazil ice crystals, with a diameter of 1.0×10^{-3} m and a boundary layer thickness of half the crystal size (0.5×10^{-3} m) (Daly, 1984). Equilibrium fractionation coefficients were taken from Lehmann and Siegenthaler (1981) ($\alpha_{\mathrm{D}} = 1.0212$ and $\alpha_{18\mathrm{O}} = 1.00291$), and diffusion coefficients from Ferrick and others (2002) (1.06×10^{-9} m^2 s^{-1} for ^{1}HD^{18}O and 1.21×10^{-9} m^2 s^{-1} for $^1\mathrm{H}_2{}^{18}$O) scaled to 0°C with the Stokes–Einstein equation from Eicken (1998). Frazil ice crystals form in episodic bursts (Smith and others, 2012). Their freezing velocities were taken from Tison and others (2001) (10^{-6} m s^{-1} and 2.7×10^{-6} m s^{-1}) and Smith and others (2012) (0.3×10^{-6} m s^{-1} to 1.4×10^{-6} m s^{-1}). Since the freezing speed (removing heavy isotopes from the liquid) is greater than the diffusion coefficient (replenishing the boundary layer with heavy isotopes), a temporary amplified depletion of heavy isotopes in the boundary layer occurs – the initial transient (Tison and others, 2001) – before the isotopic concentration equals steady state. This effect is taken into account by the model since it could be especially significant in the growth of small ice crystals (mm size). Lack of empirical data on frazil ice crystal isotopic composition makes it impossible to validate the model and quantify the error. However, the frazil ice boundary-layer freezing model is very sensitive to the assumed boundary layer thickness, which in turn depends on the crystal size. Observed frazil ice crystal sizes vary between 0.035×10^{-3} m and 4.5×10^{-3} m (Morse and Richard, 2009). Since the size class distribution of marine ice frazil ice crystals is still poorly known (e.g. Galton-Fenzi and others, 2012), this model focuses on the typical size chosen by Tison and others (2001).

In this study, the model is run for two scenarios: marine ice formation from (1) frazil ice crystals only and (2) frazil ice crystals with an estimated 15% pore space on average, similar to the average pore space Tison and others (2001) calculated for the Ronne Ice Shelf (Oerter and others, 1992) based on heat conduction and accumulation rate. The pore water is taken as pure sea water fractionating at equilibrium. Even though it remains unknown whether pore water would be merely trapped between frazil ice crystals or fractionate upon freezing to become solid marine ice, similar to river and lake ice (Ferrick and others, 2002), the modelled effective fractionation coefficient would decrease slightly if the pore water was not fractionating (by 0.44‰ for $\alpha_{18\mathrm{O}}$ and by 3.18‰ for α_{D} for marine ice with 15% sea-water-filled pores). Previous efforts to model boundary-layer freezing of marine or sea ice have focused on the oxygen isotope and salinity signal (Eicken, 1998; Tison and others, 2001). However, the reasons for variations in marine ice salinity are poorly understood (Tison and others, 2001). Even though δD is not an independent tracer, this study models the composition of both water isotopes in marine ice to allow for comparison with the measured co-isotopic signal.

RESULTS

In this section we first present the occurrence of banded, granular and mixed ice facies in marine ice from all three SMIS sites. Secondly, the variation of the δ^{18}O and δD ratios in all marine ice cores is described and co-isotopic

https://doi.org/10.3189/2015JoG14J095 Published online by Cambridge University Press

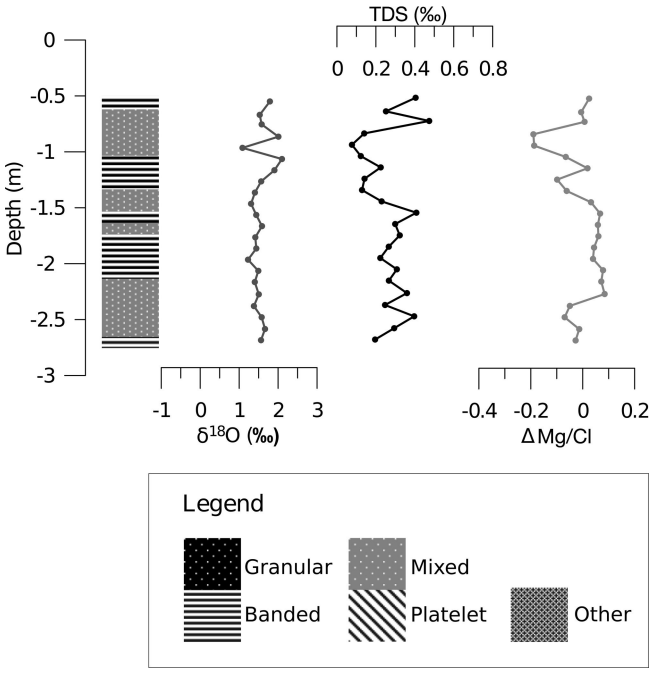

Fig. 3. Marine ice crystal facies, $\delta^{18}O$, salinity (TDS) and ΔMg/Cl ion ratio for core C5.

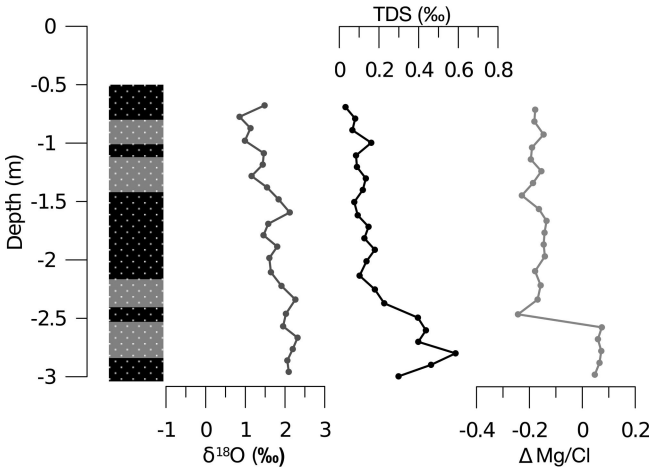

Fig. 4. Marine ice crystal facies, $\delta^{18}O$, salinity (TDS) and ΔMg/Cl ion ratio for core C9. Legend in Figure 3.

relationships are given. Subsequently, the calculated effective isotopic fractionation coefficients, which help to determine theoretical marine ice source water composition, are presented for different freezing speeds. Finally, we give marine ice salinity (TDS) and ion ratios (ΔMg/Cl and ΔK/Mg) indicating ion fractionation during freezing of marine ice pores.

Ice crystal facies of marine ice

The marine ice cores are almost entirely made up of banded and granular ice facies, including a mixed ice facies of these two crystal types that occurs in all three ice cores (Table 3; Figs 3–5). Ice core C15 shows a high percentage of both pure granular (32%) and pure banded ice crystals (24%) (Fig. 5; Table 3). The two shorter ice cores (C5 and C9), however, show an exclusive preference for either pure banded ice crystals (45%) in the case of C5 (Fig. 3; Table 3) or pure granular ice crystals (58%) in the case of C9 (Fig. 4; Table 3). Platelet ice facies are uncommon in marine ice at SMIS and make up <10% of the ice facies in C15 (Fig. 5; Table 3).

Isotopic composition of marine ice

Isotopic values in all the ice cores range from –0.43‰ to 2.29‰ $\delta^{18}O$ and –3.80‰ to 17.61‰ δD (Figs 3–6). The isotopic range increases with total core length (Figs 3–5); in the shallowest core, C5 (2.65 m long), the $\delta^{18}O$ range is 1.06‰, while $\delta^{18}O$ ranges are 1.50‰ in C9 (3.04 m long) and 2.40‰ in the longest ice core, C15 (9.44 m long). In the two shallower cores C5 and C9 (Table 3), collected close to each other (Fig. 1), the data are on average more enriched in heavy isotopes (>1.6‰ $\delta^{18}O$) than in core C15 (0.47‰ $\delta^{18}O$) (Table 3). In C9 and C15 the $\delta^{18}O$ signal shows a linear trend with depth, although the trend is positive in C9 ($r = 0.86$; Fig. 4) and negative in C15 ($r = –0.59$; Fig. 5). The $\delta^{18}O$ and δD signals are significantly correlated in all cores ($r > 0.93$), with an overall slope of 8.68 ± 0.13 ($r = 0.97$) in a co-isotopic plot (Fig. 6). Furthermore, all marine ice samples at SMIS are enriched in heavy isotopes with respect to sea water and there is a wide overlapping range of isotope values for the different ice facies (Fig. 6).

Effective fractionation coefficients

Calculating the effective fractionation coefficients for frazil ice crystals using Tison and others' (2001) model at variable freezing speeds shows that a change in freezing speed can theoretically cause an isotopic range of ≤1.55‰ $\delta^{18}O$ (Table 4; Fig. 7a). This range becomes slightly smaller when pores that fractionate at equilibrium are considered (Table 4; Fig. 7b). In either case the calculated effective fractionation coefficient for oxygen isotopes is at least 0.60‰ lower than the equilibrium fractionation coefficient (Table 4).

Salinity and ion ratios of marine ice

Marine ice collected from SMIS is slightly saline (0.03–1.01‰ TDS; Figs 3–5), with an average of 0.25‰ TDS. Similar to the isotope record, the TDS record increases

Table 3. Average marine ice chemical composition and occurrence of ice crystal facies (bd: banded; gr: granular; mx: mixed; pl: platelet; oth: other), in each SMIS marine ice core

Ice core	Length	*n*	$\delta^{18}O$	δD	TDS	ΔMg/Cl	ΔK/Mg	bd	gr	mx	pl	oth
	m		‰	‰	‰	%	%	%	%	%	%	%
C15	9.44	89	0.47 ± 0.48	2.42 ± 3.88	0.29 ± 0.18	$–9.21 \pm 5.15$	28.86 ± 12.96	24	32	32	6	2
C9	3.04	23	1.64 ± 0.43	12.43 ± 3.38	0.20 ± 0.15	$–13.64 \pm 13.14$	20.87 ± 11.09	–	58	42	–	–
C5	2.65	22	1.63 ± 0.24	13.90 ± 1.37	0.26 ± 0.11	$–0.83 \pm 7.89$	14.26 ± 5.82	45	–	55	–	–

https://doi.org/10.3189/2015JoG14J095 Published online by Cambridge University Press

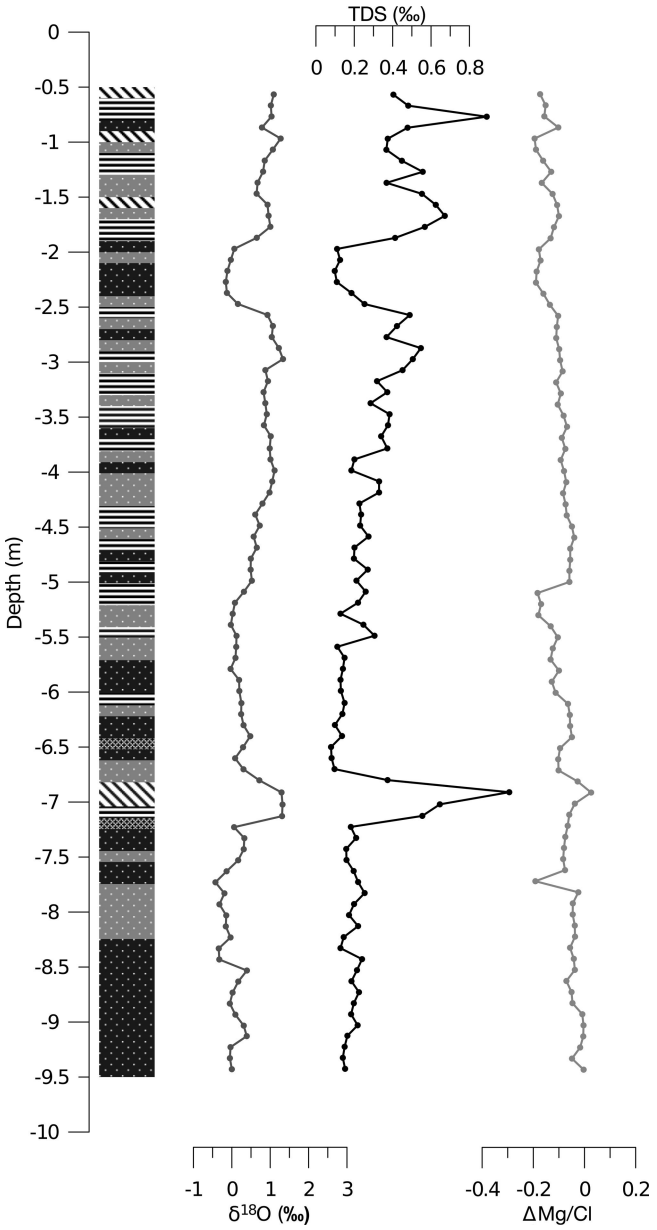

Fig. 5. Marine ice crystal facies, $\delta^{18}O$, salinity (TDS) and ΔMg/Cl ion ratio for core C15. Legend in Figure 3.

Table 4. Calculated effective fractionation coefficients (quoted as ice–water fractionation constants in ‰, i.e. $\alpha - 1$) using Tison and others' (2001) boundary layer freezing model considering different frazil ice freezing speeds (taken from Tison and others, 2001; Smith and others, 2012). Two different scenarios are considered: marine ice formation from frazil ice crystals only ('no pores') and marine ice formation from 85% frazil ice crystals with 15% of pure sea water consolidating at equilibrium freezing speed in the remaining pore spaces ('pores')

Freezing speed	$\alpha_{18O}-1$		$\alpha_{D}-1$	
$\times 10^{-6}$ m s^{-1}	pores	no pores	pores	no pores
equilibrium fractionation	2.91		21.20	
0.3	2.32	2.22	16.24	15.37
1	1.57	1.33	10.62	8.76
1.4	1.34	1.07	9.09	6.95
2.7	1.01	0.67	6.90	4.37

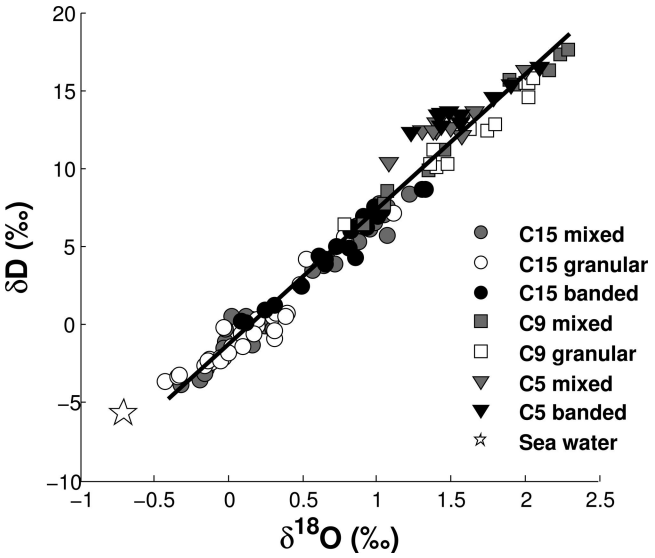

Fig. 6. Co-isotopic diagram for marine ice samples classified by ice facies from all SMIS sampling sites, plotted together with local sea water (taken as Shallow Ice Shelf Water from below the Ross Ice Shelf (Jacobs and others, 1985; Fitzsimons and others, 2012)). The slope for the linear regression for isotopic data from all ice cores together is 8.68 ± 0.13 ($r = 0.97$). Individually data from C15 have a slope of 7.92 ± 0.17 ($r = 0.98$), from C9 have a slope of 7.69 ± 0.29 ($r = 0.99$) and from C5 have a slope of 5.26 ± 0.48 ($r = 0.93$).

significantly with depth in C9 ($r = 0.83$) and decreases with depth in C15 ($r = 0.48$). Indeed, TDS and the oxygen isotope record are significantly positively correlated in C9 and C15 ($r > 0.54$). However, in C5 there is no significant linear relationship between isotopes and TDS. Samples of banded and granular ice facies occur within the whole range of measured salinities and isotopic compositions (Fig. 8a). Nonetheless, there is an apparent difference in the mean isotopic composition and salinity of different ice facies in C15; banded ice facies are more isotopically enriched and more saline than granular and mixed ice facies (Fig. 8b). Similarly, the granular ice facies in C9 are less saline than the mixed ice facies (Fig. 8b). However, there is no significant difference between the chemical compositions of different ice facies; the standard deviations of mean chemical composition for different ice facies overlap (Fig. 8b).

The marine ice at SMIS is depleted in ΔMg/Cl and enriched in ΔK/Mg (Table 3). Increases in the ΔMg/Cl signal coincide with increases in the TDS record in all cores (e.g. increase of ~0.20‰ TDS and ~0.30 ΔMg/Cl at 2.5 m in C9; Fig. 4). The ΔMg/Cl and TDS signal in C5 and C9 are positively correlated ($r > 0.64$). No significant relationship, however, exists between the ΔMg/Cl ratio and TDS in C15.

DISCUSSION

Here we first present the evidence for marine ice formation from frazil ice crystals that nucleate in supercooled water. Applying Tison and others' (2001) boundary layer freezing model, the isotopic composition of the marine ice water source is calculated using effective fractionation coefficients. Subsequently, we evaluate the evidence for marine ice formation from a changing mixed water source rather than a constant water source with a changing freezing rate. Finally, we discuss the possible geographic origin of the relatively fresher water needed in the frazil ice formation

https://doi.org/10.3189/2015JoG14J095 Published online by Cambridge University Press

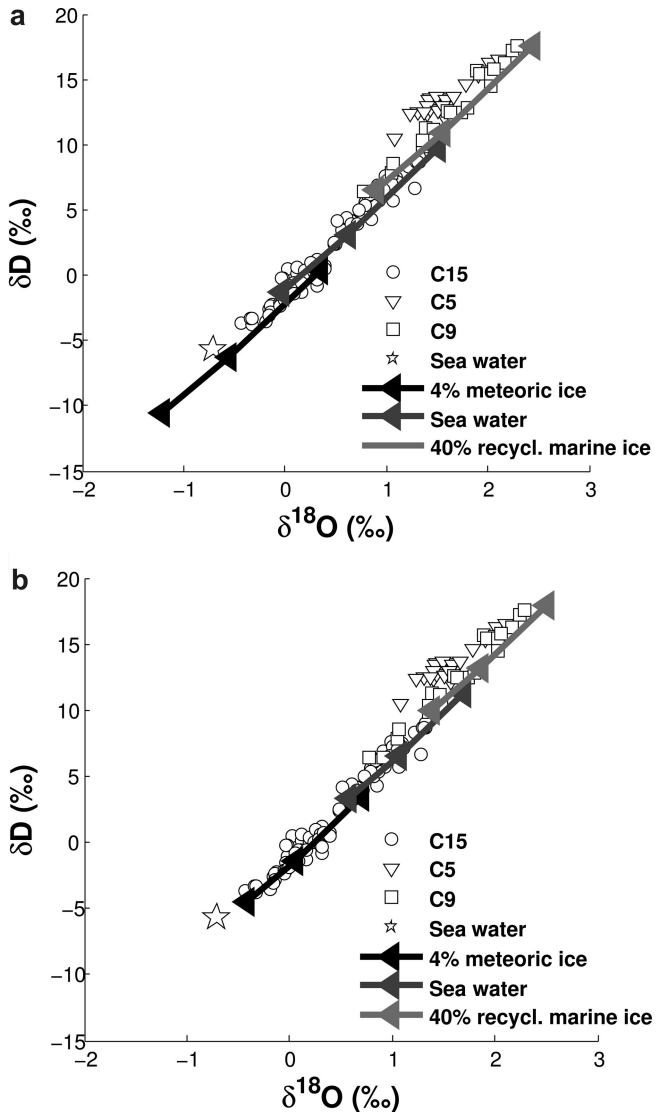

Fig. 7. $\delta^{18}O$ and δD composition of measured marine ice samples plotted together with the calculated $\delta^{18}O$ and δD composition of marine ice applying Tison and others' (2001) effective fractionation coefficients to a pure sea-water source (dark grey line) or a mixed water source of sea water and melted meteoric ice (4%: black line) or marine ice (40%: light grey line) using a range of different freezing rates. The triangles within the grey shaded lines denote calculated marine ice isotopic compositions generated at different freezing rates (2.7×10^{-6} m s^{-1}, 1×10^{-6} m s^{-1} and 0.3×10^{-6} m s^{-1}), whereby marine ice formed at a faster freezing rate remains isotopically more similar to the source water. Meteoric ice is taken as the average isotopic composition of meteoric ice samples collected from the surface of SMIS (–30.00‰ $\delta^{18}O$ and –238.27‰ δD; $n = 22$) and marine ice is defined as the measured average isotopic composition of samples from the isotopically most enriched ice core C5. (a) assumes 100% frazil ice crystals; (b) assumes 85% frazil ice crystals and 15% pores frozen from pure sea water at equilibrium fractionation.

process and what this implies with regard to marine ice formation mechanisms.

Marine ice formation from frazil ice crystals

The presence of predominantly banded and granular ice facies (Table 1) in marine ice at SMIS strongly suggests that this marine ice was formed from predominantly frazil ice crystals (e.g. Tison and others, 1993; Treverrow and others, 2010) which nucleate from supercooled water. Marine ice formation solely from the advancement of a freezing front and associated formation of columnar ice crystals (e.g. Zotikov and others, 1980) is indeed rare (Table 1) and no columnar ice crystal facies have been observed in thin sections from SMIS. Further evidence for SMIS frazil ice formation from supercooled water is provided by a higher $\delta D/\delta^{18}O$ ratio in marine ice from C5 and C9 than is predicted by the output of Tison and others' (2001) source model (Fig. 7a and b). This enrichment in δD could result from an enhanced diffusivity of deuterium in saline waters (Horita, 2009) together with a fast freezing speed, which is thought to amplify kinetic effects (Souchez and others, 2000). This is in keeping with Souchez and others (1995), who suggested using a 2‰ higher equilibrium fractionation coefficient to explain the higher enrichment of δD in marine ice.

Marine ice might not be made up of frazil ice crystals alone since these generally expel all salt during their formation (Tison and others, 1993) and SMIS marine ice is slightly saline (Table 2). Ion fractionation in SMIS marine ice samples (depletion in ΔMg/Cl and enrichment in ΔK/Mg; Table 3) also suggests the presence of sea water in pore spaces between frazil ice crystals. Nonetheless it is difficult to estimate the percentage of sea-water filled pores from its chemistry since marine ice pore water salinity and desalination processes are poorly understood. No brine channels have ever been observed in marine ice, and evidence of brine pockets was only found in the lower tens of metres of the ~200 m thick marine ice layer (which is still in hydraulic connection with the ocean) at the Amery Ice Shelf (Craven and others, 2004; Treverrow and others, 2010).

Isotopic evidence of a changing water source

Whether marine ice was formed from pure frazil ice crystals only or from a combination of frazil ice crystals and frozen pore water, the isotopic record of marine ice predominantly reflects the source water composition of frazil ice crystals. The measured isotopic range and co-isotopic slope of all SMIS marine ice samples indicate frazil ice formation from a mixed water source that changes over time. Even though the measured $\delta^{18}O$ range for samples from all ice cores at SMIS (2.71‰ $\delta^{18}O$ and 21.41‰ δD; Fig. 6) is similar to the theoretical maximum isotopic shift at equilibrium fractionation from a constant water source (Table 4), results obtained by applying Tison and others' (2001) boundary layer freezing model indicate that the isotopic composition of marine ice should only vary by $\leq$1.55‰ $\delta^{18}O$ and $\leq$11.00‰ δD considering a range of measured freezing rates for frazil ice crystals and a constant water source (no pore water; Fig. 7a; Table 4). If pores filled with sea water that fractionates upon consolidation are present, the isotopic range of marine ice formed at variable typical freezing speeds will be even smaller (1.31‰ $\delta^{18}O$ and 9.34‰ δD) (15% pore water; Fig. 7b; Table 4). Hence, the measured isotopic range of marine ice samples at SMIS indicates a source water composition that is likely not constant over time and in space, assuming an open reservoir in the ice-shelf cavity. This idea is further supported by a high co-isotopic regression slope of 8.68 ± 0.13 ($r = 0.97$) (Fig. 6), which is steeper than a freezing slope (i.e. water formed from the same water source with a variable freezing speed) in an open or closed system (Jouzel and Souchez, 1982; Souchez and Jouzel, 1984). However, since frazil ice crystals form in a water plume in the ice-shelf cavity, closed system freezing is precluded. Nonetheless, the highest

https://doi.org/10.3189/2015JoG14J095 Published online by Cambridge University Press

possible freezing slope in an open system is theoretically only 7.38, applying Souchez and Jouzel's (1984) freezing model to a water source of pure sea water taken as Shallow Ice Shelf Water (SISW) below the Ross Ice Shelf (Jacobs and others, 1985; Fitzsimons and others, 2012). Freezing slopes of sea water with a constant contribution of melted meteoric ice would be even lower. Co-isotopic mixing slopes for ice formed from a changeable water source, however, would be higher, ~8 (Souchez and Groote, 1985), which is more similar to the measured slope of all SMIS samples (Fig. 6).

For individual ice cores the isotopic range is smaller and co-isotopic slopes are shallower (Fig. 6). While the co-isotopic slope of 7.92 ± 0.17 in C15 with an isotopic range of 2.4‰ $\delta^{18}O$ remains similar to a mixing slope, the two shallower ice cores C5 and C9 have a slope ≤ 7.69 with a smaller isotopic range ($\leq$1.50‰ $\delta^{18}O$). This could suggest that the source water was similar during accretion events amounting to ~3 m of marine ice at the core sites of the shallower ice cores, extracted close to each other (Fig. 1), while the source water composition at the C15 site could have changed over the course of accreting ~9.5 m of marine ice due to the co-isotopic slope close to 8 and an isotopic range >1.55‰ $\delta^{18}O$. The low slope of 5.26 ± 0.48 in co-isotopic data from C5 is lower than a freezing slope, even if the source water was mainly glacial water derived from meteoric ice. The isotopic range of 1.06‰ $\delta^{18}O$ with most samples clustering tightly around 1.5‰ $\delta^{18}O$ (Fig. 6) might be too small to allow for a representative freezing or mixing slope.

Since there is some evidence that marine ice at SMIS partially formed from consolidation of sea-water filled pores, an increase in marine ice salinity is consistent with slower consolidation rates of frazil ice crystals. A significant correlation between the TDS and ΔMg/Cl signal in C5 and C9 could therefore suggest that sea-water filled pores consolidate more slowly (leading to higher ion fractionation) when salinity is high.

Source water composition

Since the crystallography provides evidence that marine ice is primarily composed of frazil ice crystals, which nucleate in supercooled water, the marine ice source water at SMIS is likely a mixture of local sea water and fresher and possibly warmer water. This combination of water masses supercools upon mixing (double diffusion mechanism) and/or adiabatic lifting (ice pump mechanism). The fresher-than-sea water could originate from melted meteoric ice (Souchez and others, 1995, 1998) and/or melted marine ice (Souchez and others, 1991; Tison and others, 1993).

Applying the calculated effective fractionation coefficients of Tison and others' (1993) model (Table 4) to sea water suggests that marine ice at SMIS with an isotopic concentration $\geq$1.70‰ $\delta^{18}O$ (Fig. 7b) could have formed from a water source with a component of recycled marine ice. The exact cut-off threshold depends on the calculated fractionation coefficient and the assumed sea-water composition. This study took SISW as measured below the Ross Ice Shelf (Jacobs and others, 1985; Fitzsimons and others, 2012) as the ambient sea water, but it remains unknown whether the pure sea water below SMIS could be more enriched in heavy isotopes (by ~0.30‰ $\delta^{18}O$). The idea of marine ice formation from a water source with a component of melted and relatively fresher recycled marine ice was first developed by Souchez and others (1991) based on marine ice that was more enriched in heavy isotopes (up to 3.20‰ $\delta^{18}O$; Table 1) than could be explained by applying the equilibrium fractionation coefficient to sea water. However, equilibrium freezing during frazil ice formation is unlikely. Since the isotopic composition of marine ice in C5 and C9 is, on average, ~2‰ more enriched in $\delta^{18}O$ than sea water, a high contribution of recycled marine ice (~40% dependent on freezing speed) to the source water is necessary to explain all the observed enriched marine ice samples (Fig. 7a and b). The exact percentage contribution of recycled marine ice, however, is difficult to determine, especially since marine ice can be repeat-recycled. Goodwin (1993) considered the possibility that $\delta^{18}O$ marine ice samples, which are not as enriched as in Souchez and others' (1991) study (i.e. only up to 1.56‰ $\delta^{18}O$; Table 1), could have formed from repeat recycling of previously formed marine ice.

Less enriched ($\leq$1.70‰ $\delta^{18}O$) marine ice samples could have formed with a small contribution of glacial water derived from meteoric ice to the marine ice water source (especially in C15; Fig. 7a and b). Since meteoric ice is very

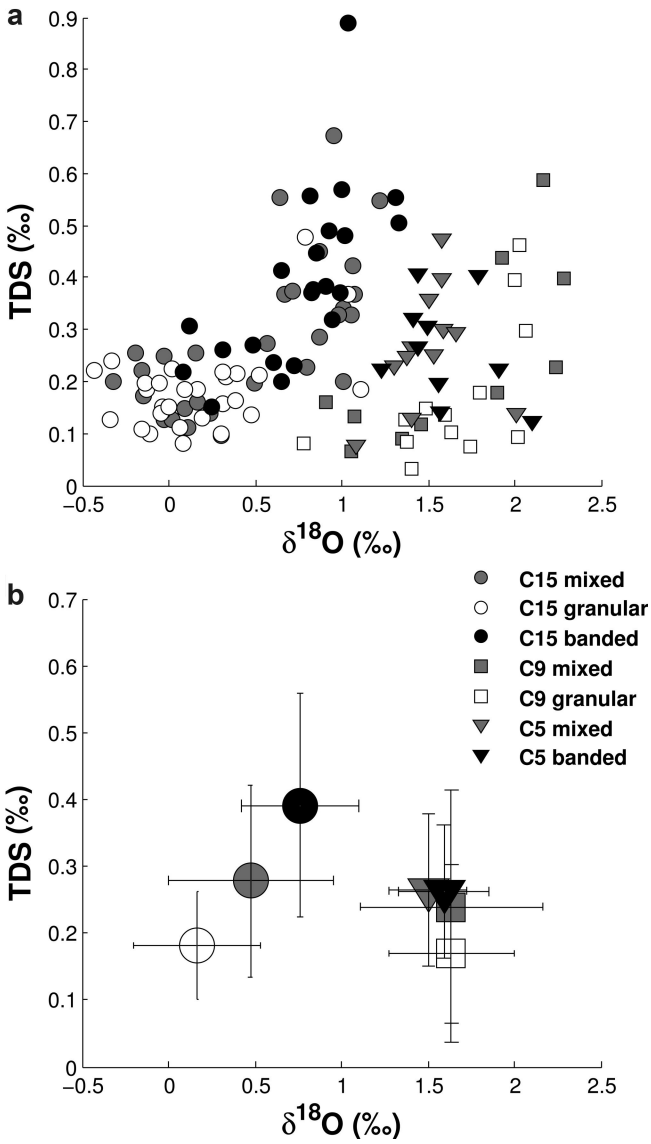

Fig. 8. Total dissolved solids (TDS) and oxygen isotopes ($\delta^{18}O$) for the different ice crystal facies in the individual ice cores. (a) Individual samples from all cores; (b) averages for all cores ± one standard deviation. Note: same key for both diagrams.

https://doi.org/10.3189/2015JoG14J095 Published online by Cambridge University Press

depleted in heavy isotopes (–35‰ to –25‰ $\delta^{18}O$; Kellogg and others, 1991a,b), a small glacial water contribution to the source water (up to a maximum of 4%) is sufficient to explain the isotopic composition of some of the less isotopically enriched and isotopically depleted ice samples in C15 (Fig. 7a and b). Previous studies interpreted the presence of a mixing slope, together with a larger isotopic range (of up to 18.00‰ $\delta^{18}O$; Table 1) than observed at SMIS of isotopically depleted samples, as the result of a mixed water source of sea water and varying proportions of melted meteoric ice (Goodwin, 1993; Souchez and others, 1995, 1998). The marine ice source water for all sample sites at SMIS, however, could consist of a mixture of all three water sources – melted meteoric ice, melted marine ice and sea water – whereby melted meteoric ice would contribute least to the mixture (in the order of 5%) due to its high isotopic depletion.

There is no evidence that different crystal morphologies are the result of marine formation from different water sources and/or proportions of pore water. There is no significant difference in the chemistry of the most common ice crystal facies (Fig. 8a); the mean isotopic signature and salinity of banded ice crystals differs only slightly from that of granular ice facies in all cores in which the standard deviations overlap (Fig. 8b).

Processes of frazil ice formation at SMIS

Here we discuss geophysical scenarios that can lead to the formation of marine ice source water as identified through the ice chemistry in the previous subsection. One possible mechanism for marine ice formation at SMIS could be the ice pump, delivering fresh water of meteoric origin to the ice-shelf cavity. This process could explain marine ice formation at site C15 where the ice likely formed from a mixed water source dominated by glacial and sea water (Fig. 7a and b). Indeed, there is a thermohaline circulation driven by either HSSW or modified Circumpolar Deep Water (mCDW) in the cavity of the adjacent Ross Ice Shelf (Dinniman and others, 2007). Ocean circulation models reveal that there is an amplified basal melt rate at the eastern margin of the Ross Ice Shelf that extends from the Ross Ice Shelf margin south past Minna Bluff (Dinniman and others, 2007; Timmermann and others, 2012). A buoyant plume of meteoric meltwater and sea water generated below the Ross Ice Shelf could enter the ice-shelf cavity of the ~300 m thinner SMIS, similar to the vertical ascent of a water plume from below the Ross Ice Shelf to the cavity of the northern McMurdo Ice Shelf (Robinson and others, 2014). Here the water in the plume would supercool due to a change in the pressure-dependent freezing point in shallower waters, and frazil ice crystals would nucleate. Potentially this water plume could also reach the ocean floor of the much shallower SMIS cavity with a maximum depth of ~400 m (Johnston and others, 2008), forming anchor ice as suggested in a modelling effort by Leonard and others (2014). However, marine ice below the Ross Ice Shelf accumulates only in a thin layer (Zotikov and others, 1980; Timmermann and others, 2012). Hence the ice pump mechanism might be not very strong in the Ross Ice Shelf cavity. Also, this ice pump would only explain the delivery of fresh water of meteoric origin into the SMIS cavity and not the recycling of marine ice.

A proportion of marine ice at SMIS shows an apparent fractionation in water isotopes that exceeds the modelled effective fractionation for freezing of frazil ice crystals from a pure sea-water source. After Souchez and others (1991) and Tison and others (1993), marine ice could be recycled in a mechanism where a shallow thermohaline or tidal circulation melts the older marine ice at depth, which then becomes supercooled upon rising to shallower waters where frazil ice crystals nucleate. However, it is unlikely that a shallow tidal circulation would reach the SMIS cavity, which is sheltered by Black and White Islands and is several tens of kilometres from the open ocean (Fig. 1).

Alternatively, marine ice at SMIS could be recycled through melting of exposed marine ice at the ice-shelf surface which would then be routed to the ice-shelf base through tide cracks. Indeed, surface melt at SMIS was observed to temporarily pool in elongated lakes between ridges of exposed marine ice during the summers of 2007 and 2010. In Figure 2 such lakes occur between the clearly distinguishable ice ridges but are frozen since the picture was taken at the start of the season. Also, a tide crack was observed to run parallel to Minna Bluff in the marine ice zone close to shore, where the ice shelf becomes regrounded. Salt deposits along the tide crack indicate that it actively connects the ice-shelf base with the ice-shelf surface. As surface meltwater would drain through the tide crack, it could become supercooled in a double-diffusion mechanism of heat and salt with the ambient sea water, whereby frazil ice crystals would nucleate. For this process to occur, both water masses, the sea water at the ice-shelf base and the recycled marine ice, need to be at their salinity-dependent freezing point and would become mixed due to local turbulence (McPhee and others, 2013). Hence, the surface meltwater would need to be cooled during percolation. In this process some refreezing could occur. Indeed, solute chemistry and ice facies of the ~9.5 m long ice core C15 show evidence of local refreezing. Between 6.8 and 7.2 m depth, for example, the marine ice salinity increases by almost an order of magnitude and the ice facies are predominantly large platelet-type crystals (Fig. 5). Similarly, platelet ice facies are present between 0.5 and 1.8 m depth together with several peaks in salinity (Fig. 5). This could be a result of surface meltwater refreezing at depth.

Recycling of ice melted at the ice-shelf surface, however, is not necessarily limited to marine ice. Water from the nearby glaciers and snowpatches on Minna Bluff close to the shore of the ice shelf (Fig. 1) could find its way into the tide cracks of SMIS and hence to the ice-shelf base. This process would be an alternative explanation for the small contribution of glacial water to the source water at SMIS, especially at site C15 (Fig. 7a and b). Recycling surface meltwater in the process of marine ice formation would imply that the ice shelf could be sustaining itself to some extent, with most of the marine ice forming during the melt season in summer. If surface ablation and local accumulation of marine ice were in equilibrium (e.g. Kellogg and others, 1990) their rates would both be in the order of ~0.1 m a^{-1}, as the measured surface ablation on SMIS (Clifford, 2005). Hence, the surface ice of the ~100 m thick SMIS would be ~1000 years old, similar to the youngest radiocarbon date of 1230 ± 50 years BP (Denton and Marchant, 2000).

Instead of recycling marine ice from the ice-shelf surface, McPhee and others (2013) suggests that loose frazil ice crystals could also be recycled in ocean turbulence before they consolidate. In this process, frazil ice crystals would be moved to deeper waters where they melt due to the pressure

https://doi.org/10.3189/2015JoG14J095 Published online by Cambridge University Press

dependence of the freezing point. Upon rising of the resulting more buoyant meltwater plume, frazil crystals would renucleate (McPhee and others, 2013). If recycling of surface meltwater or loose frazil crystals occurs below SMIS, turbulence must occur at the ice-shelf base to allow for vertical mixing. In the absence of a thermohaline and tidal circulation, it still remains to be determined how this vertical turbulence would be initiated.

There is little evidence that suggests different marine ice formation processes lead to different ice crystal facies at SMIS. Banded ice crystals are slightly more enriched in heavy isotopes and saline than the granular ice facies, especially in samples from C15 (Fig. 8a and b), but this difference is not statistically significant. Tison and others (1993) found a similarly weak chemical difference between the two ice facies but suggested that banded ice facies were generated by frazil ice crystals that aligned in a sub-ice-shelf current, whereas granular ice crystal facies were thought to result from fast frazil ice formation in a deeper thermohaline circulation further inland. In contrast, Treverrow and others (2010) found that banded ice crystal facies merely occurred in younger marine ice than granular ice crystals. This would suggest a change in crystal morphology over time. Indeed, ice deformation experiments showed that due to post-depositional ice growth and recrystallization processes associated with ice flow, the original ice crystal morphology is often altered (Wilson and others, 2014) and predominantly granular/less elongated ice crystals develop in marine ice (Dierckx and others, 2014).

CONCLUSION

The aims of this study were to determine the composition and origin of water masses of marine ice at SMIS. We have focused our analysis on the crystal morphology and the chemistry of the ice and used a boundary layer freezing model to derive the source water composition. The specific conclusions are:

SMIS marine ice was mainly formed by frazil ice crystals since the ice is almost entirely composed of granular and banded ice crystal facies.

The source water composition of SMIS marine ice is not constant but changes spatio-temporally. This is indicated by a co-isotopic mixing slope of ~8 and an isotopic range of 2.71‰ $\delta^{18}O$ and 21.41‰ δD for all marine ice samples from all sites, which is almost double the isotopic range predicted by the boundary layer freezing model for marine frazil ice formed from a constant water source at different freezing speeds.

Marine ice samples, which are isotopically depleted compared to modelled marine frazil ice formed from pure sea water, have likely formed from a source water mixture of sea water and a relatively small proportion (~4%) of melted meteoric ice. This isotopically depleted melted meteoric ice could have been vertically advected from the ice-shelf base of the adjacent ~300 m thicker Ross Ice Shelf in an ice pump mechanism.

Marine ice samples, which are isotopically enriched compared to modelled marine frazil ice formed from pure sea water, have likely formed from a source water mixture of sea water and a large proportion (~40%) of isotopically enriched melted marine ice. The exact percentage varies with freezing speed and the number of freeze–thaw–refreeze cycles. In a proposed recycling mechanism, marine ice, which is exposed at the ice-shelf surface, melts and drains through the tide crack to the ice-shelf base, where it becomes turbulently mixed with relatively colder and saltier sea water and frazil ice crystals nucleate in a double diffusion process. Thus, summer surface melt could make a substantial contribution to basal ice-shelf mass accretion particularly at the southern margin of SMIS.

Consequently we conclude that basal boundary conditions and the formation of marine ice at the relatively thin SMIS are at least partially determined by surface meltwater generation. The proposed mechanism of marine ice recycling thus ties together surface and basal processes, and could potentially slow ice-shelf disintegration.

ACKNOWLEDGEMENTS

We thank Antarctica New Zealand for excellent logistical support on SMIS. Sean Fitzsimons held a University of Otago Research Grant and Inka Koch was supported by a University of Otago Doctoral Scholarship. The New Zealand Royal Society Mobility Fund, the Antarctic Science Bursary and the University of Otago Polar Environments research theme provided financial support to establish collaboration with the Laboratoire de Glaciologie in Belgium. We thank Jono Conway, Nicolas Cullen, Michael Hambrey, Abigail Lovett, Martin Sharp, Simon Shelton and Nita Smith for help with the ice-core extraction in the field. For assistance with scientific instruments in the laboratory and cold room we are grateful to Julie Clark, Saïda El Amri, Marie Dierckx and Robert van Hale. We thank Eric Roulin for help in reviving the numerical code for the boundary layer freezing model of frazil ice crystals. Inga Smith and Sarah Mager made helpful suggestions on an earlier version of the manuscript. We thank three anonymous reviewers for comments which helped to improve the clarity of the paper.

REFERENCES

Banwell AF, Caballero M, Arnold NS, Glasser NF, Mac Cathles L and MacAyeal DR (2014) Supraglacial lakes on the Larsen B ice shelf, Antarctica, and at Paakitsoq, West Greenland: a comparative study. *Ann. Glaciol.*, **55**(66), 1–8 (doi: 10.3189/2014AoG66A049)

Berkman PA and Forman S (1996) Pre-bomb radiocarbon and the reservoir correction for calcareous marine species in the Southern Ocean. *Geophys. Res. Lett.*, **23**, 363–365 (doi: 10.1029/96GL00151)

Bindschadler RP and 17 others (2011) Getting around Antarctica: new high-resolution mappings of the grounded and freely-floating boundaries of the Antarctic ice sheet created for the International Polar Year. *Cryosphere*, **5**(3), 569–588 (doi: 10.5194/tc-5-569-2011)

Bombosch A and Jenkins A (1995) Modeling the formation and deposition of frazil ice beneath Filchner–Ronne Ice Shelf. *J. Geophys. Res.*, **100**(C4), 6983–6992 (doi: 10.1029/94JC03224)

Burton JA, Prim RC and Slichter WP (1953) The distribution of solute in crystals grown from the melt. 1. Theoretical. *J. Chem. Phys.*, **21**(11), 1987–1991 (doi: 10.1063/1.1698728)

Clifford AE (2005) Physiography, flow characteristics and vulnerability of the Southern McMurdo Ice shelf, Antarctica. (MSc thesis, University of Otago)

https://doi.org/10.3189/2015JoG14J095 Published online by Cambridge University Press

Craven M and 6 others (2004) Initial borehole results from the Amery Ice Shelf hot-water drilling project. *Ann. Glaciol.*, **39**, 531–539 (doi: 10.3189/172756404781814311)

Craven M and 7 others (2005) Borehole imagery of meteoric and marine ice layers in the Amery Ice Shelf, East Antarctica. *J. Glaciol.*, **51**(172), 75–84 (doi: 10.3189/172756505781829511)

Craven M, Allison I, Fricker HA and Warner R (2009) Properties of a marine ice layer under the Amery Ice Shelf, East Antarctica. *J. Glaciol.*, **55**(192), 717–728 (doi: 10.3189/002214309789470941)

Daly SF (1984) Frazil ice dynamics. *CRREL Monogr.* 84-1

Debenham F (1919) A new mode of transportation by ice: the raised marine muds of South Victoria Land (Antarctica). *Q. J. Geol. Soc.*, **75**(2), 51–76 (doi: 10.1144/GSL.JGS.1919.075.01-04.08)

Denton GH and Marchant DR (2000) The geologic basis for a reconstruction of a grounded ice sheet in McMurdo Sound, Antarctica, at the Last Glacial Maximum. *Geogr. Ann. A*, **82**(2–3), 167–211 (doi: 10.1111/j.0435-3676.2000.00121.x)

Depoorter MA and 6 others (2013) Calving fluxes and basal melt rates of Antarctic ice shelves. *Nature*, **502**(7469), 89–92 (doi: 10.1038/nature12567)

Dierckx M and Tison J-L (2013) Marine ice deformation experiments: an empirical validation of creep parameters. *Geophys. Res. Lett.*, **40,** 134–138 (doi: 10.1029/2012GL054197)

Dierckx M, Peternell M, Schroeder C and Tison J-L (2014) Influence of the pre-existing microstructure on the mechanical properties of marine ice during compression experiments. *J. Glaciol.*, **60**(221), 576–586 (doi: 10.3189/2014JoG13J154)

Dinniman MS, Klinck JM and Smith WO (2007) Influence of sea ice cover and icebergs on circulation and water mass formation in a numerical circulation model of the Ross Sea, Antarctica. *J. Geophys. Res*, **112**(C11), C11013 (doi: 10.1029/2006JC004036)

Dupont TK and Alley RB (2005) Assessment of the importance of ice-shelf buttressing to ice-sheet flow. *Geophys. Res. Lett.*, **32**(4), L04503 (doi: 10.1029/2004GL022024)

Durand G, Gagliardini O, Thorsteinsson T, Svensson A, Kipfstuhl S and Dahl-Jensen D (2006) Ice microstructure and fabric: an up-to-date approach for measuring textures. *J. Glaciol.*, **52**(179), 619–630 (doi: 10.3189/172756506781828377)

Eicken H (1994) Structure of under-ice melt ponds in the central Arctic and their effect on the sea-ice cover. *Limnol. Oceanogr.*, **39**(3), 682–693 (doi: 10.4319/lo.1994.39.3.0682)

Eicken H (1998) Deriving modes and rates of ice growth in the Weddell Sea from microstructural, salinity and stable-isotope data. In Jeffries MO ed. *Antarctic sea ice physical processes, interactions and variability*. (Antarctic Research Series 74) American Geophysical Union, Washington, DC, 89–122 (doi: 10.1029/AR074p0089)

Eicken H, Oerter H, Miller H, Graf W and Kipfstuhl J (1994) Textural characteristics and impurity content of meteoric and marine ice in the Ronne Ice Shelf, Antarctica. *J. Glaciol.*, **40**(135), 386–398

Ferrick MG, Calkins DJ, Perron NM, Cragin JH and Kendall C (2002) Diffusion model validation and interpretation of stable isotopes in river and lake ice. *Hydrol. Process.*, **16**(4), 851–872 (doi: 10.1002/hyp.374)

Fitzsimons S (1997) Entrainment of glaciomarine sediments and formation of thrust-block moraines at the margin of Sørsdale Glacier, East Antarctica. *Earth Surf. Process. Landf.*, **22**, 175–187

Fitzsimons S, Mager S, Frew R, Clifford A and Wilson G (2012) Formation of ice-shelf moraines by accretion of sea water and marine sediment at the southern margin of the McMurdo Ice Shelf, Antarctica. *Ann. Glaciol.*, **53**(60), 211–220 (doi: 10.3189/2012AoG60A155)

Foldvik A and Kvinge T (1974) Conditional instability of sea water at its freezing point. *Deep-Sea Res.*, **21**, 169–174 (doi: 10.1016/0011-7471(74)90056-4)

Fricker HA, Popov S, Allison I and Young N (2001) Distribution of marine ice beneath the Amery Ice Shelf. *Geophys. Res. Lett.*, **28**(11), 2241–2244 (doi: 10.1029/2000GL012461)

Galton-Fenzi BK, Hunter JR, Coleman R, Marsland SJ and Warner RC (2012) Modeling the basal melting and marine ice accretion of the Amery Ice Shelf. *J. Geophys. Res.: Oceans*, **117**(C9), C09031 (doi: 10.1029/2012JC008214)

Goodwin ID (1993) Basal ice accretion and debris entrainment within the coastal ice margin, Law Dome, Antarctica. *J. Glaciol.*, **39**(131), 157–166

Gow AJ and Epstein S (1972) Use of stable isotopes to trace origins of ice in a floating ice tongue. *J. Geophys. Res.*, **77**(33), 6552–6557 (doi: 10.1029/JC077i033p06552)

Gow AJ, Weeks WF, Hendrickson G and Rowland R (1965) New light on the mode of uplift of the fish and fossiliferous moraines of the McMurdo Ice Shelf, Antarctica. *J. Glaciol.*, **5**(42), 813–828

Horita J (2009) Isotopic evolution of saline lakes in the low-latitude and polar regions. *Aquat. Geochem.*, **15**(1–2), 43–69 (doi: 10.1007/s10498-008-9050-3)

Hubbard B, Tison J-L, Pattyn F, Dierckx M, Boereboom T and Samyn D (2012) Optical-televiewer-based identification and characterization of material facies associated with an Antarctic ice-shelf rift. *Ann. Glaciol.*, **53**(60), 137–146 (doi: 10.3189/2012AoG60A045)

Jacobs SS, Fairbanks RG and Horibe Y (1985) Origin and evolution of water masses near the Antarctic continental margin: evidence from $H_2{}^{18}O/H_2{}^{16}O$ ratios in seawater. In Jacobs SS ed. *Oceanology of the Antarctic Continental Shelf*. (Antarctic Research Series 43) American Geophysical Union, Washington, DC, 59–85 (doi: 10.1029/AR043)

Jacobs SS, Helmer HH, Doake CSM, Jenkins A and Frolich RM (1992) Melting of ice shelves and the mass balance of Antarctica. *J. Glaciol.*, **38**(130), 375–387

Jansen D, Luckman A, Kulessa B, Holland PR and King EC (2013) Marine ice formation in a suture zone on the Larsen C Ice Shelf and its influence on ice shelf dynamics. *J. Geophys. Res.*, **118**(3)**,** 1628–1640 (doi: 10.1002/jgrf.20120)

Johnston L and 6 others (2008) Cenozoic basin evolution beneath the southern McMurdo Ice Shelf, Antarctica. *Global Planet. Change*, **62**(1–2), 61–76 (doi: 10.1016/j.gloplacha.2007.11.004)

Joughin I and Vaughan DG (2004) Marine ice beneath the Filchner–Ronne Ice Shelf, Antarctica: a comparison of estimated thickness distributions. *Ann. Glaciol.,* **39,** 511–517 (doi: 10.3189/172756404781814717)

Jouzel J and Souchez RA (1982) Melting–refreezing at the glacier sole and the isotopic composition of the ice. *J. Glaciol.*, **28**(98), 35–42

Kellogg TB, Kellogg DE and Stuiver M (1990) Late Quaternary history of the southwestern Ross Sea: evidence from debris bands on the McMurdo Ice Shelf, Antarctica. In Bentley CR ed. *Contributions to Antarctic research I*. (Antarctic Research Series 50**)** American Geophysical Union, Washington, DC, 25–56 (doi: 10.1029/AR050)

Kellogg TB, Kellogg DE and Stuiver M (1991a) Oxygen isotope data from the McMurdo Ice Shelf, Antarctica: implications for debris band formation and glacial history. *Antarct. J. US*, **26**(5), 73–76

Kellogg TB, Kellogg DE and Stuiver M (1991b) Radiocarbon dates from the McMurdo Ice Shelf, Antarctica: implications for debris band formation and glacial history. *Antarct. J. US*, **26**(5), 77–79

Khazendar A, Tison J-L, Stenni B, Dini M and Bondesan A (2001) Significant marine-ice accumulation in the ablation zone beneath an Antarctic ice shelf. *J. Glaciol.*, **47**(158), 359–368 (doi: 10.3189/172756501781832160)

Khazendar A, Rignot E and Larour E (2009) Roles of marine ice, rheology, and fracture in the flow and stability of the Brunt/Stancomb-Wills Ice Shelf. *J. Geophys. Res.*, **114**(F4), F04007 (doi: 10.1029/2008JF001124)

Kulessa B, Jansen D, Luckman AJ, King EC and Sammonds PR (2014) Marine ice regulates the future stability of a large Antarctic ice shelf. *Nature Commun.*, **5**, 3707 (doi: 10.1038/ncomms4707)

Lehmann M and Siegenthaler U (1991) Equilibrium oxygen-isotope and hydrogen-isotope fractionation between ice and water. *J. Glaciol.*, **37**(125), 23–26 (doi: 10.1021/j100856a060)

Leonard GH, Mager SM, Pauling A, Hughes KG and Smith IJ (2014) Towards a process model for predicting potential anchor ice

formation sites in coastal Antarctic Waters. *J. Spatial Sci.,* **59**(2), 297–312 (doi: 10.1080/14498596.2014.913271)
Lewis EL and Perkin RG (1986) Ice pumps and their rates. *J. Geophys. Res.*, **91**(C10), 1756–1762 (doi: 10.1029/JC091iC10p11756)
Mager S, Smith IJ, Kempema EW, Thomson BJ and Leonard GH (2013) Anchor ice in polar oceans. *Progr. Phys. Geogr.*, **37**(4), 468–483 (doi: 10.1177/0309133313479815)
Martin S (1981) Frazil ice in rivers and oceans. *Ann. Rev. Fluid Mech.*, **13**, 379–397 (doi: 10.1146/annurev.fl.13.010181.002115)
Martin S and Kauffman P (1974) The evolution of under-ice melt ponds, or double diffusion at the freezing point. *J. Fluid Mech.*, **64,** 507–527 (doi: 10.1017/S0022112074002527)
Maus S and 7 others (2011) Ion fractionation in young sea ice from Kongsfjorden, Svalbard. *Ann. Glaciol.*, **52**(57), 301–310 (doi: 10.3189/172756411795931804)
McMahon KL and Lackie MA (2006) Seismic reflection studies of the Amery Ice Shelf, East Antarctica: delineating meteoric and marine ice. *Geophys. J. Int.*, **166**(2), 757–766 (doi: 10.1111/j.1365-246X.2006.03043.x)
McPhee MG, Skogseth R, Nilsen F and Smedsrud LH (2013) Creation and tidal advection of a cold salinity front in Storfjorden: 2. Supercooling induced by turbulent mixing of cold water. *J. Geophys. Res.: Oceans*, **118**(8), 3737–3751 (doi: 10.1002/jgrc.20261)
Millero FJ, Feistel R, Wright DG and McDougall TJ (2008) The composition of Standard Seawater and the definition of the Reference-Composition Salinity Scale. *Deep-Sea Res. I*, **55**(1), 50–72 (doi: 10.1016/j.dsr.2007.10.001)
Monaghan AJ, Bromwich DH, Powers JG and Manning KW (2005) The climate of the McMurdo, Antarctica, region as represented by one year of forecasts from the Antarctic Mesoscale Prediction System. *J. Climate*, **18**(8), 1174–1189 (doi: 10.1175/JCLI3336.1)
Moore JC, Reid AP and Kipfstuhl J (1994) Microstructure and electrical-properties of marine ice and its relationship to meteoric ice and sea-ice. *J. Geophys. Res.*, **99**(C3), 5171–5180 (doi: 10.1029/93JC02832)
Morgan VI (1972) Oxygen isotope evidence for bottom freezing on Amery Ice Shelf. *Nature*, **238**(5364), 393–394 (doi: 10.1038/238393a0)
Morse B and Richard M (2009) A field study of suspended frazil ice particles. *Cold Reg. Sci. Technol.*, **55**(1), 86–102 (doi: 10.1016/j.coldregions.2008.03.004)
Oerter H and 6 others (1992) Evidence for basal marine ice in the Filchner–Ronne Ice Shelf. *Nature*, **358**(6385), 399–401 (doi: 10.1038/358399a0)
Pattyn F and 8 others (2012) Melting and refreezing beneath Roi Baudouin Ice Shelf (East Antarctica) inferred from radar, GPS, and ice core data. *J. Geophys. Res.: Earth Surf.*, **117**(F4), F04008 (doi: 10.1029/2011JF002154).
Robinson NJ, Williams MJM, Stevens CL, Langhorne PJ and Haskell TG (2014) Evolution of a supercooled Ice Shelf Water plume with an actively growing subice platelet matrix. *J. Geophys. Res.: Oceans*, **119**, 3425–3446 (doi: 10.1002/2013JC009399)
Smith IJ, Langhorne PJ, Frew RD, Vennell R and Haskell TG (2012) Sea ice growth rates near ice shelves. *Cold Reg. Sci. Technol.*, **83–84**, 57–70 (doi: 10.1016/j.coldregions.2012.06.005)
Souchez RA and Groote JM (1985) δD–$\delta^{18}O$ relationships in ice formed by subglacial freezing: paleoclimatic implications. *J. Glaciol.*, **31**(109), 229–232
Souchez R and Jouzel J (1984) On the isotopic composition in δD and $\delta^{18}O$ of water and ice during freezing. *J. Glaciol.*, **30**(106), 369–372
Souchez R and 8 others (1991) Ice composition evidence of marine ice transfer along the bottom of a small Antarctic ice shelf. *Geophys. Res. Lett.*, **18**(5), 849–852 (doi: 10.1029/91GL01077)
Souchez R and 6 others (1995) Investigating processes of marine ice formation in a floating ice tongue by a high-resolution isotopic study. *J. Geophys. Res.*, **100**(C4), 7019–7025 (doi: 10.1029/95JC00142)
Souchez R, Khazendar A, Ronveaux D and Tison J-L (1998) Freezing at the grounding line in East Antarctica: possible implications for sediment export efficiency. *Ann. Glaciol.,* **27**, 316–320
Souchez R, Jouzel J, Lorrain R, Sleewaegen S, Stievenard M and Verbeke V (2000) A kinetic isotope effect during ice formation by water freezing. *Geophys. Res. Lett.*, **27**(13), 1923–1926 (doi: 10.1029/2000GL006103)
Swithinbank C (1970) Ice movement in the McMurdo Sound area of Antarctica. *IAHS Publ.* 86 (Symposium at Hanover 1968 – *Antarctic Glaciological Exploration (ISAGE)*), 472–487
Timmermann R, Wang Q and Hellmer HH (2012) Ice-shelf basal melting in a global finite-element sea-ice/ice-shelf/ocean model. *Ann. Glaciol.*, **53**(60), 303–314 (doi: 10.3189/2012AoG60A156)
Tison J-L, Ronveaux D and Lorrain RD (1993) Low-salinity frazil ice generation at the base of a small Antarctic ice shelf. *Antarct. Sci.*, **5**(3), 309–322 (doi: 10.1017/S0954102093000409)
Tison J-L, Khazendar A and Roulin E (2001) A two-phase approach to the simulation of the combined isotope/salinity signal of marine ice. *J. Geophys. Res.*, **106**(C12), 31 387–31 401 (doi: 10.1029/2000JC000207)
Treverrow A, Warner RC, Budd WF and Craven M (2010) Meteoric and marine ice crystal orientation fabrics from the Amery Ice Shelf, East Antarctica. *J. Glaciol.*, **56**(199), 877–890 (doi: 10.3189/002214310794457353)
Warren SG, Roesler CS and Brandt RE (1997) Solar radiation processes in the East Antarctic sea ice zone. *Antarct. J. US*, **32,** 185–187
Wen JH, Wang YF, Wang WL, Jezek KC, Liu HX and Allison I (2010) Basal melting and freezing under the Amery Ice Shelf, East Antarctica. *J. Glaciol.*, **56**(195), 81–90 (doi: 10.3189/002214310791190820)
Wilson CJL, Peternell M, Piazolo S and Luzin V (2014) Microstructure and fabric development in ice: lessons learned from in situ experiments and implications for understanding rock evolution. *J. Struct. Geol.*, **61**, 50–77 (doi: 10.1016/j.jsg.2013.05.006)
Zotikov IA, Zagorodnov VS and Raikovsky JV (1980) Core drilling through the Ross Ice Shelf (Antarctica) confirmed basal freezing. *Science*, **207**(4438), 1463–1464 (doi: 10.1126/science.207.4438.1463)

MS received 19 June 2014 and accepted in revised form 1 May 2015